



This is a repository copy of *Numerical and experimental studies of excitation force approximation for wave energy conversion*.

White Rose Research Online URL for this paper:  
<http://eprints.whiterose.ac.uk/129115/>

Version: Accepted Version

---

**Article:**

Guo, B., Patton, R.J., Jin, S. et al. (1 more author) (2018) Numerical and experimental studies of excitation force approximation for wave energy conversion. *Renewable Energy*, 125. pp. 877-889. ISSN 0960-1481

<https://doi.org/10.1016/j.renene.2018.03.007>

---

**Reuse**

This article is distributed under the terms of the Creative Commons Attribution-NonCommercial-NoDerivs (CC BY-NC-ND) licence. This licence only allows you to download this work and share it with others as long as you credit the authors, but you can't change the article in any way or use it commercially. More information and the full terms of the licence here: <https://creativecommons.org/licenses/>

**Takedown**

If you consider content in White Rose Research Online to be in breach of UK law, please notify us by emailing [eprints@whiterose.ac.uk](mailto:eprints@whiterose.ac.uk) including the URL of the record and the reason for the withdrawal request.



[eprints@whiterose.ac.uk](mailto:eprints@whiterose.ac.uk)  
<https://eprints.whiterose.ac.uk/>

# Numerical and Experimental Studies of Excitation Force Approximations for Wave Energy Conversion

Bingyong Guo<sup>a</sup>, Ron J. Patton<sup>a,\*</sup>, Siya Jin<sup>a</sup>, Jianglin Lan<sup>a</sup>

<sup>a</sup>*School of Engineering and Computer Science, University of Hull, Cottingham Road, Hull, UK, HU6 7RX*

---

## Abstract

Past or/and future information of the excitation force is useful for real-time power maximisation control of Wave Energy Converter (WEC) systems. Current WEC modelling approaches assume that the wave excitation force is accessible and known. However, it is not directly measurable for oscillating bodies. This study aims to provide reasonably accurate approximations of the excitation force for the purpose of enhancing the effectiveness of WEC control. In this work, three approaches are proposed to approximate the excitation force, by (i) identifying the excitation force from wave elevation, (ii) estimating the excitation force from the measurements of pressure, acceleration and displacement and (iii) observing the excitation force via an unknown input observer. These methods are compared with each other to discuss their advantages, drawbacks and application scenarios. To validate and compare the performance of the proposed methods, a 1/50 scale heaving point absorber WEC has been tested in a wave tank under variable wave scenarios. The experimental data are in accordance with the excitation force approximations in both the frequency- and time-domains based upon both regular and irregular wave excitation. Hence, the proposed excitation force approximation approaches have great potential for WEC power maximisation via real-time control.

*Keywords:* excitation force modelling, model verification, wave energy

---

\*Corresponding author

*Email addresses:* B.Guo@2013.hull.ac.uk (Bingyong Guo), R.J.Patton@hull.ac.uk (Ron J. Patton), S.Jin@2015.hull.ac.uk (Siya Jin), lanjianglin@126.com (Jianglin Lan)

## 1. Introduction

To harvest green power from the ocean waves, more than 1,000 concepts of wave energy conversion have been proposed [1]. Various technologies and devices for wave energy conversion are detailed in [2, 3, 4]. Recent research focuses on the power maximisation control of various Wave Energy Converters (WECs) [5], including reactive control [6], latching control [7], declutching control [8], Model Predictive Control (MPC) [9, 10] and etc. For some of these power maximisation control strategies, the excitation force information is compulsory and essential. Some of these strategies, e.g. MPC, even depend on excitation force prediction. However, the excitation force is not directly measurable for oscillating WECs. Thus, the estimation of the excitation force with reasonable accuracy is critical for some real-time power maximisation control of WEC systems.

In the literature, considering the regular wave conditions, the excitation force is modelled in a generic way using analytical approaches. As described in [11], the excitation force is represented by the integral of the pressure over the **wetted surface** of floating structures. This gives a good estimation of the excitation force but it is not implementable for moving structures in offshore environment. Also for some specific geometries there are appropriate analytical formulae that provide relatively precise excitation force estimation [12]. These approaches assume the phase shift of the excitation force with respect to the incident wave is zero for harmonic waves, thereby rendering these excitation force modelling approaches applicable for numerical WEC simulation. However, these approaches are inappropriate for generating reference information for real-time control implementations since the excitation force is not directly measurable for oscillating structures.

For irregular wave conditions, the excitation force can be approximated using a superposition assumption in terms of the well-known Frequency Response Function (FRF) [13]. Excitation force estimation is useful for assessing both the

29 wave energy resource as well as the WEC dynamics and control performance.  
30 What is the drawback? This approach does not easily relate the excitation force  
31 estimation to physical measurements, e.g incident wave elevation or pressure  
32 acting on the **wetted surface** of the oscillating structure. Hence, once again it  
33 is difficult to obtain time-varying reference signals for real-time WEC control  
34 using this strategy.

35 However, several studies focus specifically on excitation force estimation or  
36 approximation for future real-time control implementation. A state-space mod-  
37 elling method of the causalised excitation force is described in [14] without  
38 discussing its realisation and performance. A potential approach to achieve the  
39 causalisation with up-stream wave measurement is mathematically discussed  
40 in [15] and has been implemented and verified experimentally in [16]. **The up-**  
41 **stream method can provide enough future information of the excitation force for**  
42 **some optimum control if the up-stream distance and direction are properly de-**  
43 **signed to overcome the irregularity of wave frequency and direction.** The study  
44 in [17] details the discrete-time identification of non-linear excitation force based  
45 on numerical wave tank simulation. Studies in [18, 19] apply the Kalman Fil-  
46 ter (KF) and Extended Kalman Filter (EKF) to estimate the excitation force.  
47 However, as discussed in [18, 19] the KF/EKF approaches require a priori knowl-  
48 edge of the process and measurement noises. **The measurement noise can be**  
49 **estimated for the characteristics of the sensors and the data acquisition systems**  
50 **whilst the process noise can be obtained from a wild rang of specially designed**  
51 **experiments.** Also the Unknown Input Observer (UIO) technique is applied to  
52 estimate the excitation **force** [20, 21]. This approach relies on the accessibility  
53 of all the system state variables, some of which are difficult to measure. All  
54 these approaches relate the excitation force approximations with real-time wave  
55 elevation or/and WEC dynamics and hence the approximations can be used  
56 for real-time control reference generation. Moreover, to gain future information  
57 of the excitation force for latching control or MPC, Auto-Regressive (AR) or  
58 Auto-Regressive-Moving-Average (ARMA) models can be applied to provide  
59 short-term prediction of the excitation force, as detailed in [22, 23].

60 The aim of the current study is to develop an excitation force estima-  
61 tion/approximation strategy with potential for real-time WEC power maxim-  
62 sation control. Three approaches are proposed:

- 63 • In the Wave-To-Excitation-Force (W2EF) approach, the excitation force  
64 is estimated from the wave elevation. This method is inspired by the  
65 causalisation concept in [14] but contributes to its the implementation,  
66 verification and performance evaluation. The causalisation is achieved via  
67 wave prediction using the W2EF method. This can be compared with the  
68 up-stream measurement approach of and realised using up-stream wave  
69 measurement according to [16]. **If the up-stream distance is large enough,**  
70 **the up-stream method in can provide enough future information of the**  
71 **excitation force for some power maximisation control strategies, such as**  
72 **MPC, latching control. The W2EF method proposed in this study only**  
73 **gives the current information of the excitation force. However, future**  
74 **information of the excitation force can also be provided by the W2EF**  
75 **method if the wave prediction horizon is large enough. This idea is quite**  
76 **similar with the up-stream method.**
- 77 • In the Pressure-Acceleration-Displacement-To-Excitation-Force (PAD2EF)  
78 method, the excitation force is derived from the WEC hull pressure mea-  
79 surements as well as the heave acceleration and displacement. Different  
80 from the excitation force identification method using pressure sensors in  
81 [16], this PAD2EF approach uses more kinds of sensors and hence has the  
82 advantage of sensing redundancy and the disadvantage of system com-  
83 plexity.
- 84 • In the Unknown-Input-Observation-of-Excitation-Force (UIOEF) technique,  
85 the excitation force is observed from an appropriately designed UIO. Com-  
86 pared to the UIO method in [20, 21], this UIOEF approach only requires  
87 the displacement measurement and hence it is more flexible in practice.  
88 The UIO design is based on an a Linear Matrix Inequality (LMI) formu-  
89 lation of an  $H_\infty$  optimisation to minimise the effect of the excitation force

derivative on the estimation error.

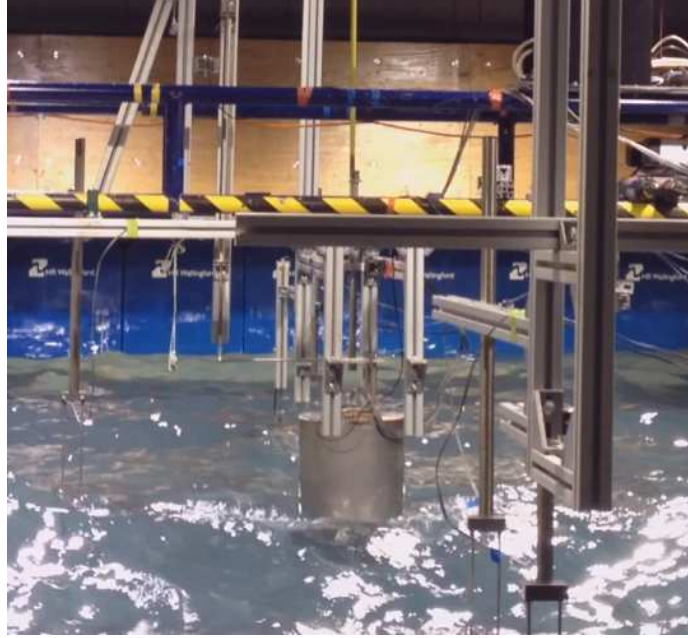


Figure 1: 1/50 scale PAWEC under wave tank test.

Table 1: Dimension of the cylindrical buoy.

Symbol	Parameter	Units	Value
$r$	buoy radius	m	0.15
$h$	buoy height	m	0.56
$d$	buoy draught	m	0.28
$M$	buoy mass	kg	19.79
$k_{hs}$	hydrostatic stiffness	N/m	693.43
$A_{\infty}$	added mass at infinite frequency	kg	6.57

91 To verify the proposed excitation force modelling approaches, a 1/50 scale  
 92 cylindrical heaving Point Absorber Wave Energy Converter (PAWEC) has been

93 designed, constructed and tested in a wave tank at the University of Hull, as il-  
 94 lustrated in Figure 1. The buoy dimensions are given in Table 1. A wide variety  
 95 of wave tank tests have been conducted under regular and irregular wave condi-  
 96 tions for verification of the three proposed W2EF, PAD2EF and UIOEF mod-  
 97 elling strategies. The experimental data show a high correspondence with the  
 98 numerical results of these approaches both in the time- and frequency-domains.  
 99 The advantages, drawbacks and application scenarios of these approaches are  
 100 also discussed in this study.

101 The paper is structured as follows. In Section 2, the modelling of the PAWEC  
 102 motion is described. Section 3 details the W2EF, PAD2EF and UIOEF ap-  
 103 proaches to estimate the excitation force in real-time. Section 4 illustrates the  
 104 wave tank tests configuration and wave conditions of the **excitation tests and**  
 105 **wave-excited-motion tests**. Numerical and experimental results are compared  
 106 and discussed in Section 5 and conclusions are drawn in Section 6.

## 107 2. Modelling of PAWEC Motion

108 Under the assumptions of ideal fluid (inviscid, incompressible and irrotat-  
 109 tional), linear wave theory and small motion amplitude, the motion of a PAWEC  
 110 obeys Newton’s second law, given in an analytical representation in [24] as:

$$M\ddot{z}(t) = F_e(t) + F_r(t) + F_{hs}(t) + F_{pto}(t). \quad (1)$$

111  $F_e(t)$ ,  $F_{hs}(t)$ ,  $F_r(t)$  and  $F_{pto}(t)$  are the excitation, radiation, hydrostatic and  
 112 Power Take-Off (PTO) forces.  $M$  is the mass of the PAWEC.  $z(t)$  is the heaving  
 113 displacement **and  $\ddot{z}$  represents the buoy acceleration in heave**. It is assumed  
 114 that friction, viscous and mooring forces are neglected here. For the sake of  
 115 simplicity, only the heave motion is investigated in this study.

116 For a vertical cylinder shown in Figure 1, the hydrostatic force is proportional  
 117 to the displacement  $z(t)$ , represented as:

$$F_{hs}(t) = -\rho g \pi r^2 z(t) = -k_{hs} z(t), \quad (2)$$

118 where  $\rho$ ,  $g$  are the water density and gravity constant, respectively.  $r$  and  
 119  $k_{hs} = \rho g \pi r^2$  represent the buoy radius and hydrostatic stiffness, respectively.

120 The radiation force  $F_r(t)$  is characterised by the added mass and radiation  
 121 damping coefficient. According to the Cummins equation [25], the radiation  
 122 force can be written in the time-domain as:

$$F_r(t) = -A_\infty \ddot{z}(t) - k_r(t) * \dot{z}(t), \quad (3)$$

123 where  $A_\infty$  and  $k_r(t)$  are the added mass at infinite frequency and the kernel  
 124 function, or so-called Impulse Response Function (IRF), of the radiation force.

125  $X * Y$  represents the convolution operation of  $X$  and  $Y$ .

126 For modelling of the excitation force  $F_e(t)$ , analytical approaches have been  
 127 developed in [11, 13]. For regular waves, an analytical representation of the  
 128 excitation force is given as [11]:

$$F_e(t) = \frac{H}{2} \left( \frac{2\rho g^3 R(\omega)}{\omega^3} \right)^{1/2} \cos(\omega t), \quad (4)$$

129 where  $H$ ,  $\omega$  and  $R(\omega)$  represent the wave height, angular frequency and radiation  
 130 damping coefficient, respectively. For irregular waves, the excitation force can  
 131 be approximated based on the superposition principle and its FRF, given in a  
 132 spectrum form in [13], as:

$$F_e(t) = \Re \left[ \sum_i \sqrt{2S(\omega_i) \Delta\omega} H_e(j\omega_i) e^{j(\omega_i t + \phi_i)} \right], \quad (5)$$

133 where  $\Delta\omega$  is the angular frequency step,  $\omega_i$  and  $\phi_i$  are the wave frequency and  
 134 random phase with subscript  $i$ .  $S(\omega_i)$  and  $H_e(j\omega_i)$  represent the wave spectrum  
 135 and the excitation force FRF, respectively.

136 The analytical representations in Eqs. (4) and (5) are widely used to assess  
 137 the power capture performance of various WEC devices. These may not be  
 138 suitable for real-time WEC control application since the excitation force is an  
 139 unknown, uncontrollable and unmeasurable external stochastic input. Hence,  
 140 the motivation for this study comes from a need to approximate/estimate the  
 141 excitation force from the given WEC measurements for the purpose of generating  
 142 suitable reference information for real-time WEC control.



143 For good WEC control performance, the challenge is that a real-time rep-  
 144 resentation of the excitation force is essential. Therefore, in many studies the  
 145 Computational Fluid Dynamics (CFD) techniques are adopted to compute the  
 146 fluid-structure interaction for WEC dynamic modelling. One should recall that  
 147 the WEC hydrodynamics are non-linear and hence the CFD analysis is compu-  
 148 tationally expensive. It is actually not straightforward to apply control strate-  
 149 gies based on CFD results without very significant effort of CFD data charac-  
 150 terisation and post-processing. An effective study that combines control and  
 151 CFD together based on OpenFOAM simulation is described in [26]. Meanwhile,  
 152 Boundary Element Method (BEM) packages, such as WAMIT<sup>®</sup>, AQWA<sup>™</sup> and  
 153 NEMOH, are applied to compute the WEC-wave interaction using efficient com-  
 154 putation. Amongst these BEM packages, NEMOH is an open source code, ded-  
 155 icated to compute first order wave loads on offshore structures [27]. It is a  
 156 suitable alternative of commercial BEM codes, like WAMIT<sup>®</sup> and AQWA<sup>™</sup>,  
 157 since it provides computation results as accurate as WAMIT<sup>®</sup> [28]. Therefore,  
 158 NEMOH is adopted in this study.

159 The radiation coefficients in Eq. (3) and the excitation force FRF in Eq.  
 160 (5) can be obtained by solving the boundary value problem in NEMOH [27].  
 161 The NEMOH simulation is based on the buoy as shown in Figure 1. The  
 162 radiation force kernel function  $k_r(t)$  is shown in Figure 2 and the excitation  
 163 force FRF (including the amplitude and phase responses) is shown in Figure 3.  
 164 In Figure 3 the amplitude response of the excitation force is normalised with  
 165 respect to the hydrostatic stiffness  $k_{hs}$  and the phase response is normalised with  
 166 respect to  $\pi$ . Since the time-domain representation is preferred for real-time  
 167 power optimisation control, Section 3 discusses the modelling or approximation  
 168 approaches of the excitation force.

### 169 3. Excitation Force Approximation Approaches

170 As described in Section 2, the excitation force FRF is available from NEMOH.  
 171 Therefore, a time-domain representation of the excitation force can be identi-

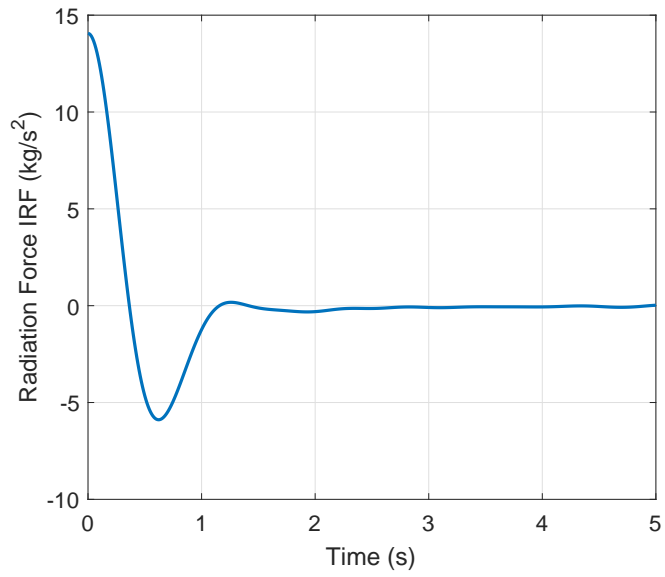


Figure 2: Kernel function of the radiation force from NEMOH.

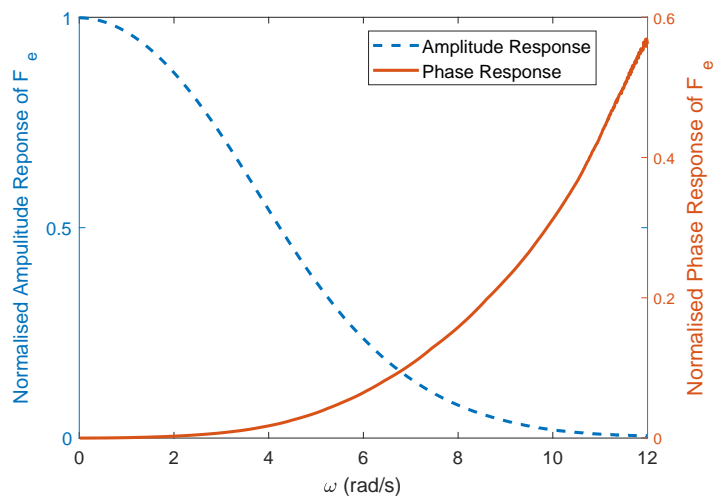


Figure 3: Amplitude and phase responses of the excitation force from NEMOH.

172 fied from its FRF if the incident wave is assumed as the input, referred to as  
 173 the W2EF method. For an oscillating device, if the pressure distribution on  
 174 the **wetted surface** and the WEC motion are measurable, the excitation force  
 175 can be estimated from these measurements as well, referred to as the PAD2EF  
 176 approach. For some WEC systems, only the oscillating displacement is accessi-  
 177 ble. In this situation, the excitation force can be estimated via UIO techniques,  
 178 referred to as the UIOEF method. These approximation approaches of the  
 179 excitation force are detailed in Sections 3.1, 3.2 and 3.3, respectively.

### 180 3.1. W2EF Modelling

#### 181 3.1.1. Outline of W2EF Method

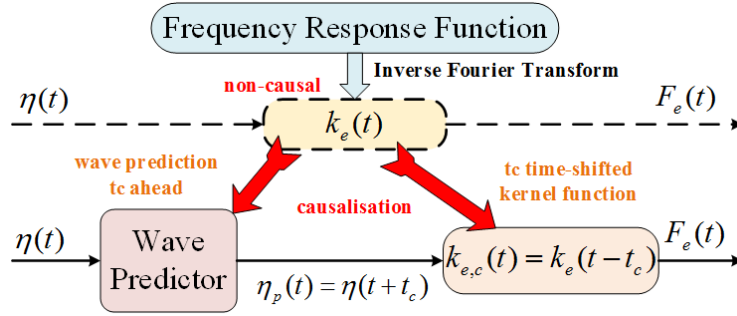


Figure 4: Schematic diagram of the W2EF modelling approach.

182 Since the frequency-domain response of the excitation force is available in  
 183 Figure 3, its time-domain kernel function  $k_e(t)$  can be gained by the inverse  
 184 Fourier transform. However, the kernel function  $k_e(t)$  characterises that the  
 185 W2EF process is non-causal. Therefore, a time-shift technique is applied to  
 186 causalise the non-causal kernel function  $k_e(t)$  to its causalised form  $k_{e,c}(t)$  (see  
 187 Figure 4) with causalisation time  $t_c$  ( $t_c \geq 0$ ). Thus, the wave elevation prediction  
 188 with  $t_c$  in advance is required. The implementation of the W2EF modelling is  
 189 detailed in this Section.

190 According to the frequency-domain response in Figure 3, the excitation force  
 191 can be represented as:

$$F_e(j\omega) = H_e(j\omega)A(j\omega), \quad (6)$$

192 where  $H_e(j\omega)$  is the FRF of the W2EF process.  $A(j\omega)$  is the frequency-domain  
 193 representation of the incoming wave elevation  $\eta(t)$ .

194 Alternatively, the excitation force can be expressed in the time-domain as:

$$F_e(t) = k_e(t) * \eta(t) = \int_{-\infty}^{\infty} k_e(t - \tau)\eta(\tau)d\tau, \quad (7)$$

195 where  $k_e(t)$  is the excitation force IRF related to its FRF  $H_e(j\omega)$ , given as:

$$k_e(t) = \frac{1}{2\pi} \int_{-\infty}^{\infty} H_e(j\omega)e^{j\omega t} d\omega. \quad (8)$$

196 Based on the frequency-domain response in Figure 3, the kernel function  
 197  $k_e(t)$  is computed according to Eq. (8) and shown in Figure 5, in which the  
 198 red solid curve (marked NEMOH IRF ( $t < 0$ )) illustrates the non-causality of  
 199 the W2EF process. The physical meaning of the non-causality is explained in  
 200 [15]. The  $k_e(t)$  values for the  $t < 0$  part are almost the same as the  $t \geq 0$  part.  
 201 Therefore, ignoring of the non-causality will in general lead to significant errors  
 in the excitation force estimation.

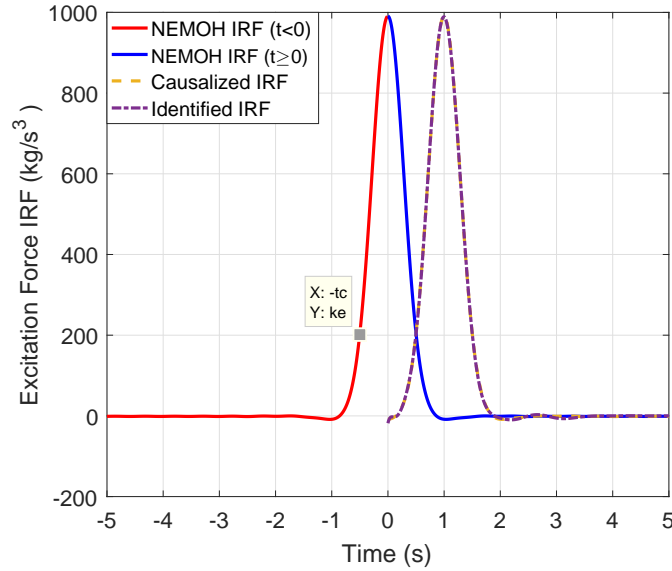


Figure 5: Comparison of the excitation force IRFs.

202

203 **To note:** In [14, 15], the kernel function  $k_e(t)$  is time-shifted first and then  
 204 treated as a curve fitting problem. However, the implementation procedure and  
 205 the results of the excitation force are not given in [14, 15]. In this study, both  
 206 the causalisation and its implementation with wave prediction are outlined in  
 207 this Section. The numerical and experimental results of the excitation force are  
 208 compared in both the time- and frequency-domains in Section 5.1.

209 As shown in Figure 4, the incident wave propagates through a non-causal sys-  
 210 tem characterised by  $k_e(t)$  and gives the excitation force approximation. How-  
 211 ever, this non-causal system is not implementable. Therefore, causalisation is  
 212 required and can be achieved with a time-shifted kernel function  $k_{e,c}(t)$  and wave  
 213 prediction  $\eta_p(t)$ . The wave prediction horizon is the same as the causalisation  
 214 time  $t_c$ .

215 According to the property of the convolution operation, this causalised sys-  
 216 tem with wave prediction gives the same excitation force of the non-causal sys-  
 217 tem [14], since:

$$F_e(t) = k_e(t) * \eta(t) \quad (9)$$

$$= k_e(t - t_c) * \eta(t + t_c) \quad (10)$$

$$= k_{e,c}(t) * \eta_p(t), \quad (11)$$

218 where

$$k_{e,c}(t) = k_e(t - t_c), \quad (12)$$

219

$$\eta_p(t) = \eta(t + t_c). \quad (13)$$

220  $k_{e,c}(t)$  and  $\eta_p(t)$  are the causalised IRF of the excitation force and the predicted  
 221 wave elevation with  $t_c$  in advance, respectively. The procedures to identify the  
 222  $k_{e,c}(t)$  and to predict the  $\eta_p(t)$  are detailed as follows.

### 223 3.1.2. System Identification of Causalised Kernel Function

224 The excitation force expressed in Eq. (11) is causal if the predicted wave  
 225 is viewed as the system input. Hence, the convolution operation can be ap-  
 226 proximated by a finite order system [14, 28, 29]. In this study, realisation

227 theory is applied to the causalised kernel function  $k_{e,c}(t)$  to approximate the  
 228 system matrices in Eqs. (14) and (15) directly with the MATLAB<sup>®</sup> function  
 229 *imp2ss* [30] from the robust control toolbox. The order number of the identi-  
 230 fied system is quite high, as determined by  $k_{e,c}(t)$ . Hence, model reduction is  
 231 required and achieved using the square-root balanced model reduction method  
 232 with MATLAB<sup>®</sup> function *balmar* [31].

233 In this study Eq. (11) is approximated by the following state-space model:

$$\dot{x}_e(t) = A_e x_e(t) + B_e \eta_p(t), \quad (14)$$

$$F_e(t) \approx C_e x_e(t), \quad (15)$$

234 where  $x_e(t) \in \mathbb{R}^{n \times 1}$  is the state vector for the excitation system.  $A_e \in \mathbb{R}^{n \times n}$ ,  
 235  $B_e \in \mathbb{R}^{n \times 1}$  and  $C_e \in \mathbb{R}^{1 \times n}$  are the system matrices.  $n$  represents the system  
 236 order number.

237 To identify the causalised system, the causalisation time  $t_c$  and the system  
 238 order number  $n$  should be selected carefully. Here a truncation error function  
 239  $E_t$  is defined to evaluate the causalisation time, given as:

$$E_t = \frac{\int_{-\infty}^{-t_c} |k_e(t)| dt}{\int_{-\infty}^{\infty} |k_e(t)| dt}. \quad (16)$$

240 For  $t_c \in [0, 5]$ , the truncation error is given in Figure 6. For  $t_c = 0.8$  s, the  
 241 truncation error is about  $E_t = 0.0104$  and for  $t_c = 2$  s, the truncation error is  
 242 about  $E_t = 0.0044$ . Increasing the causalisation time can decrease the trunca-  
 243 tion error. However, the truncation error is small enough for  $t_c \in [0.8, 2]$ . Thus  
 244  $t_c = 0.8 : 0.05 : 2$  s is selected to determine the system order number  $n$ .

245 To further determine the causalisation time  $t_c$  and the system order  $n$ , a  
 246 fitting-goodness function (called *FG*) of the causalised IRF  $k_{e,c}(t)$  is defined  
 247 with a cost-function of Normalized Mean Square Error (NMSE), as:

$$FG = 1 - \left\| \frac{x_{ref} - x}{x_{ref} - \bar{x}_{ref}} \right\|_2^2, \quad (17)$$

248 where  $\|X\|_2^2$  and  $\bar{X}$  are the 2-norm and mean value of vector  $X$ , respectively.  
 249 The fitting-goodness tends to 1 for the best fitting and  $-\infty$  for the worst fitting.

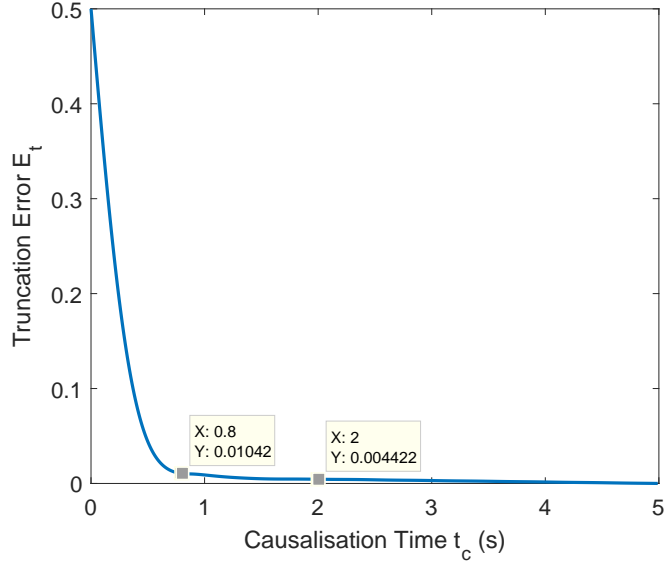


Figure 6: Truncation error of the excitation force IRF varies against the causalisation time.

250 The fitting-goodness of the causalised excitation IRF relies on the causali-  
 251 sation time  $t_c$  and system order number  $n$ . Figure 7 shows the fitting-goodness  
 252 function varying with the causalisation time  $t_c = 0.8 : 0.05 : 2$  s and the system  
 253 order number  $n = 3 : 1 : 8$ . For a constant  $t_c$ , the fitting-goodness increases as  
 254 the system order number  $n$  increases. To achieve a perfect fitting or identifica-  
 255 tion (such as a given fitting-goodness  $FG \geq 0.98$ ), a larger causalisation time  
 256 requires a higher system order number  $n$ . For instance,  $n = 4$  gives  $FG \geq 0.98$   
 257 for  $t_c = 1$  s and  $n = 5$  is required to achieve  $FG \geq 0.98$  for  $t_c = 1.2$  s.

258 According to Figures 6 and 7, a system with  $t_c = 1$  s and  $n = 6$  gives a low  
 259 truncation error ( $E_t < 0.01$ ) and a good fitting of the causalised kernel function  
 260  $k_{e,c}(t)$  ( $FG > 0.99$ ). Hence  $t_c = 1$  s and  $n = 6$  are selected for this study.  
 261 The identified IRF is compared with the causalised and original IRFs of the  
 262 excitation force in Figure 5. **To note,  $t_c = 1$  s is selected here to overcome the**  
 263 **non-causality of the W2EF process and to provide current information of the**  
 264 **excitation force. Future information of the excitation force can be obtained via**

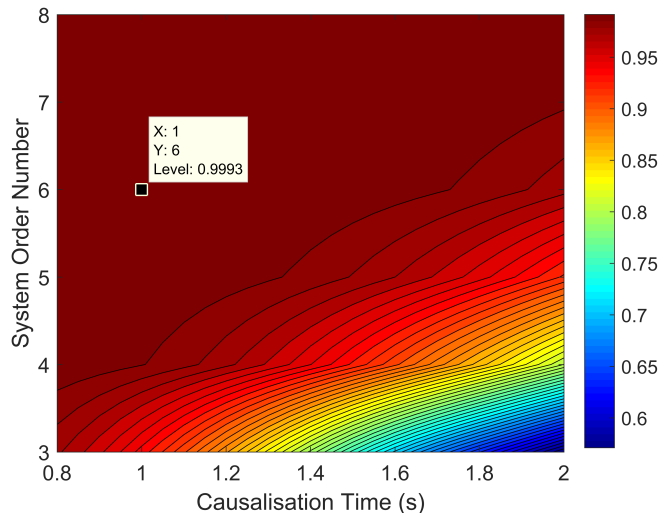


Figure 7: Fitting-goodness with varying causalisation time  $t_c$  and system order number  $n$ .

265 **excitation force prediction or increasing the wave prediction horizon.**

### 266 3.1.3. Wave Prediction

267 According to Eq. (10), a short-term wave prediction is required to achieve  
 268 the causalisation problem in Figure 4. There are several approaches to provide  
 269 reasonably accurate wave prediction for a short-term horizon, the notable of  
 270 which are: (i) the AR model approach [22], (ii) the ARMA model approach [23]  
 271 and (iii) the fast Fourier transform approach [32]. The real-time implementation  
 272 of wave prediction is discussed in [33]. In [22], wave prediction via AR model  
 273 shows a high accordance to the ocean waves in Irish sea. Since these techniques  
 274 are mature, the AR model approach developed in [22] is adopted in this study  
 275 to provide a short-term wave prediction.

276 For harmonic waves, wave prediction is easy to achieve. For irregular waves,  
 277 three campaigns of wave prediction practice using AR model are shown in Fig-  
 278 ure 4. The wave elevation  $\eta(t)$  is acquired from wave tank tests and satisfies  
 279 the Pierson-Moskowitz (PM) spectrum [34] with peak frequency  $f_p = 0.4, 0.6,$   
 280 **0.8 Hz.** As suggested in [22], a low pass filter has been applied to the wave



281 elevation measurements for improving the prediction performance. The wave  
 282 prediction horizon is the same as the causalisation time  $t_c$  and this is expressed  
 283 in Eq. (10). According to Figure 7,  $t_c = 1$  s is selected for the excitation force  
 approximation.

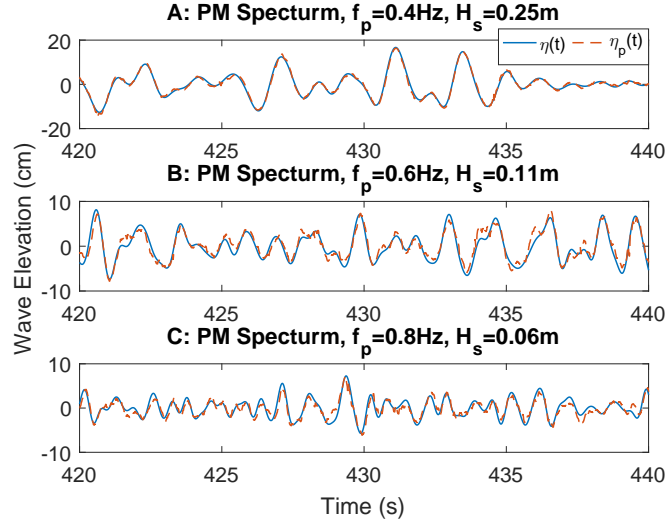


Figure 8: Comparison of wave elevations between the experimental measurements and the numerical predictions under irregular wave conditions.

284  
 285 For wave tank tests, the sampling frequency is 100 Hz and hence the predic-  
 286 tion horizon is 100 for  $t_c = 1$  s. The AR model order number is determined by  
 287 the goodness-of-fit index defined in [22] and hence the order number is selected  
 288 as 120 to keep the goodness-of-fit index larger than 70%. The order number  
 289 is large due to the high sampling frequency and hence it can be reduced by  
 290 decreasing the sampling frequency. For each campaign of wave tank tests, the  
 291 experimental data of 600 s are collected and divided into two parts equally. The  
 292 first part of data ( $t = 0 : 0.01 : 300$  s) are used to estimate the AR model  
 293 parameters and the second part of data ( $t = 300 : 0.01 : 600$  s) are used for  
 294 model verification. This study focuses on the verification of the W2EF method  
 295 and the AR model parameters are computed off-line. However, the real-time  
 296 on-line wave prediction can be achieved [33]. It can be seen from Figure 8

297 that the predicted wave elevation fits the experimental data well. However, the  
 298 prediction performance decreases as the peak frequency increases. For the PM  
 299 spectrum, higher peak frequency results in wider bandwidth and hence one po-  
 300 tential way to improve the prediction performance is to increase the order of  
 301 the AR model when the peak frequency is high. In this study the AR model  
 302 is adopted as a wave predictor to provide future information for the identified  
 303 system, as shown in Figure 4.

### 304 3.2. PAD2EF Modelling

#### 305 3.2.1. Outline of PAD2EF Method

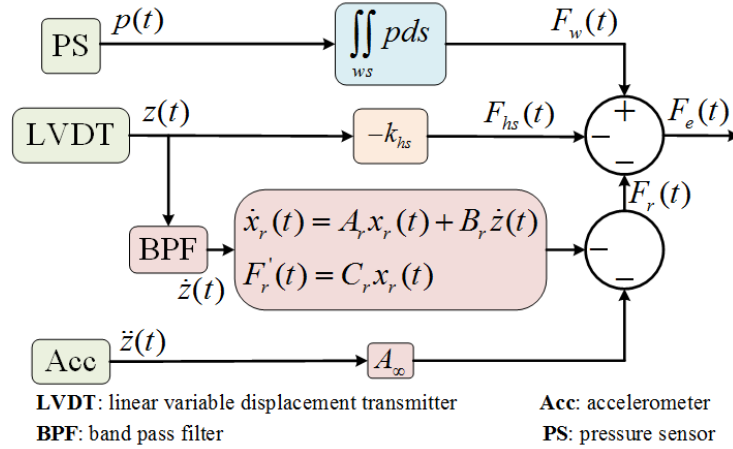


Figure 9: Schematic diagram of the PAD2EF modelling approach.

306 For an oscillating PAWEC, the excitation force can be reconstructed from its  
 307 sensing system. As shown in Figure 9, the total wave force  $F_w(t)$  acting on the  
 308 structure can be estimated from the pressure measurement  $p(t)$  on the **wetted**  
 309 **surface**. The hydrostatic force defined in Eq. (2) can be represented by the  
 310 displacement measurement  $z(t)$ . The radiation force can be approximated from  
 311 the measurements of the velocity  $\dot{z}(t)$  and acceleration  $\ddot{z}(t)$ . **The acceleration**  
 312 **measurement is post-processed with low pass filter since this study focuses on the**  
 313 **PAD2EF method verification rather than real-time implementation.** Therefore,

314 the excitation force can be approximated as:

$$F_e(t) = F_w(t) - F_{hs}(t) - F_r(t). \quad (18)$$

315 The convolution term of the radiation force  $F_r(t)$  in Eq. (3) is approximated  
316 by a finite order system [29] as follows.

### 317 3.2.2. Radiation Force Approximation

318 The convolution operation of the radiation force in Eq. (3) is defined as a  
319 radiation subsystem, given as:

$$F'_r(t) = k_r(t) * \dot{z}(t). \quad (19)$$

320 The kernel function  $k_r(t)$  is gained from NEMOH and shown in Figure 2. The  
321 convolution approximation approach is the same as described in Section 3.1.2.

322 To determine an appropriate system order number, the fitting-goodness func-  
323 tion in Eq. (17) is applied. A third order system is adopted to approximate the  
324 radiation subsystem in Eq. (19) with a fitting-goodness of  $FG = 0.9989$ , as:

$$\dot{x}_r(t) = A_r x_r(t) + B_r \dot{z}(t), \quad (20)$$

$$F'_r(t) \approx C_r(t) x_r(t), \quad (21)$$

325 where  $x_r(t) \in \mathbb{R}^{3 \times 1}$  is the state vector for the radiation system.  $A_r \in \mathbb{R}^{3 \times 3}$ ,  
326  $B_r \in \mathbb{R}^{3 \times 1}$  and  $C_r \in \mathbb{R}^{1 \times 3}$  are the system matrices. Therefore, the excitation  
327 force can be estimated from the measurements of the pressure, acceleration and  
328 displacement, given as:

$$F_e(t) = \iint p(t) ds + k_{hs} z(t) + A_\infty \ddot{z}(t) + F'_r(t). \quad (22)$$

### 329 3.2.3. Pseudo-Velocity Measurement

330 As shown in Figure 9, the measurements of the pressure, displacement and  
331 acceleration are accessible and implementable. However, the velocity measure-  
332 ment is difficult and expensive to obtain. A “pseudo-velocity” can be esti-  
333 mated/observed from the displacement/acceleration measurements. In [19], the  
334 velocity is obtained from the first order derivative of an accurate displacement

335 measurement with a high sampling frequency. The drawbacks of this approach  
 336 are: (i) the velocity estimation is infected by the measurement noise and (ii) the  
 337 velocity estimation is always one sample period behind the real velocity (high  
 338 sampling frequency is required).

339 In this work, a carefully designed Band-Pass Filter (BPF) is applied to obtain  
 340 the velocity estimate from the displacement measurement. Compared with the  
 341 differentiation approach, a velocity estimate with less phase lag can be gained  
 342 via the BPF. The second order BPF is given as:

$$BPF(s) = \frac{A_{bpf} \frac{\omega_c}{Q_{bpf}} s}{s^2 + \frac{\omega_c}{Q_{bpf}} s + \omega_c^2}, \quad (23)$$

343 where  $A_{bpf}$  is the amplitude gain at the central frequency  $\omega_c$  and  $Q_{bpf}$  is the  
 344 quality factor. The drawbacks of this BPF method are: (i) the velocity es-  
 345 timation is influenced by measurement noise and (ii) the BPF is difficult to  
 346 implement with analogue filter. However, the BPF is applicable in a software  
 347 digital filtering way. Additionally, the velocity can be observed via an appro-  
 348 priately designed observer and this part of work is detailed in Section 3.3.3.

349 A variety of wave tank tests are conducted under irregular wave conditions  
 350 and the comparison of the pseudo-velocity measurements between the differen-  
 351 tial, BPF and observation methods is given in Figure 10. The pseudo-velocity  
 352 measurements via these three methods shows a high accordance to each other  
 353 due to: (i) the sampling frequency (100 Hz) is very large compared with the wave  
 354 frequency (1.2 Hz) and (ii) the displacement measurement is accurate enough.  
 355 The differential method requires high sampling frequency and accurate displace-  
 356 ment measurement. The BPF approach calls for large  $A_{bpf}$  and  $Q_{bpf}$  and this  
 357 may result in instability of the closed-loop control system. The third method of  
 358 observing the velocity is preferred since the observer design is easy, robust and  
 359 flexible to implement.

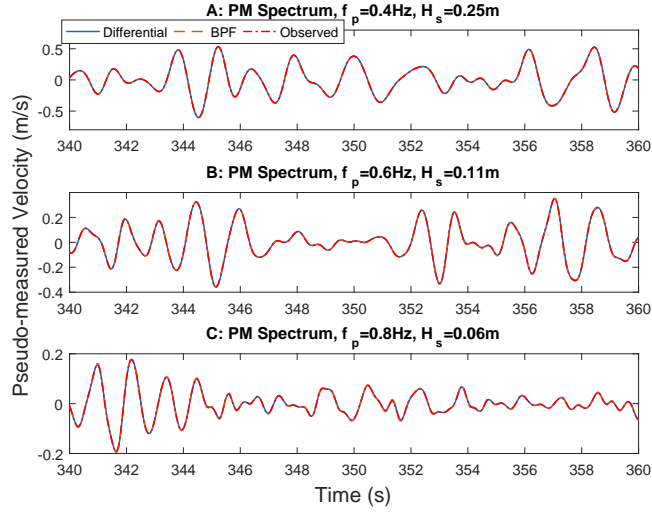


Figure 10: Comparison of pseudo-measured velocity under irregular wave conditions.

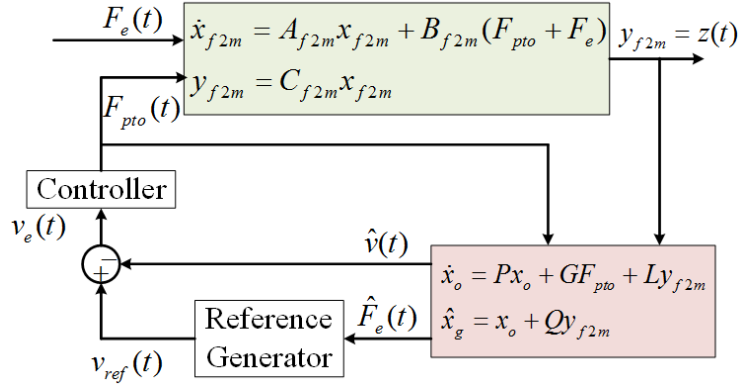


Figure 11: Schematic diagram of the UIOEF modelling approach.

360 *3.3. UIOEF Modelling*

361 *3.3.1. Outline of UIOEF Method*

362 As the convolution term of the radiation force in Eq. (19) is approximated  
 363 by a state-space model in Eqs. (20) and (21), the PAWEC motion under the  
 364 wave excitation can be represented in a state-space form. Therefore, an appro-  
 365 priately designed UIO can be applied to estimate the unknown excitation force.  
 366 As shown in Figure 11, a generic UIO is applied to estimate the excitation  
 367 force and buoy velocity from the displacement measurement. The estimated  
 368 excitation force is used to generate the velocity reference, whilst the estimated  
 369 velocity is viewed as the velocity measurement to provide feedback for the con-  
 370 troller. However, this study focuses on the UIO estimator design rather than on  
 371 the controller structure and design. This method is referred to as the UIOEF  
 372 modelling method.

373 *3.3.2. Force-To-Motion Modelling*

374 According to Eq. (1), the PAWEC starts to oscillate under the stimulation  
 375 of the excitation and PTO forces. The PAWEC motion with excitation force  
 376 input is defined as the Force-To-Motion (F2M) model. Considering the radiation  
 377 approximation in Eqs. (20) and (21), the F2M model is re-written as:

$$x_{f2m} = [z \quad \dot{z} \quad x_r]^T, \quad (24)$$

$$\dot{x}_{f2m}(t) = A_{f2m}x_{f2m}(t) + B_{f2m}F_e(t) + B_{f2m}F_{pto}(t), \quad (25)$$

$$y_{f2m}(t) = C_{f2m}x_{f2m}(t), \quad (26)$$

378 with

$$A_{f2m} = \begin{bmatrix} 0 & 1 & 0 \\ -\frac{k_{hs}}{M_t} & 0 & -\frac{C_r}{M_t} \\ 0 & B_r & A_r \end{bmatrix}, \quad (27)$$

$$B_{f2m} = \begin{bmatrix} 0 & -\frac{1}{M_t} & 0 \end{bmatrix}^T, \quad (28)$$

$$C_{f2m} = \begin{bmatrix} 1 & 0 & 0 \end{bmatrix}, \quad (29)$$

379 where  $M_t = M + A_\infty$  represents the total mass.  $x_{f2m}(t) \in \mathbb{R}^{5 \times 1}$  is the F2M  
 380 state vector.  $A_{f2m} \in \mathbb{R}^{5 \times 5}$ ,  $B_{f2m} \in \mathbb{R}^{5 \times 1}$  and  $C_{f2m} \in \mathbb{R}^{1 \times 5}$  are the system  
 381 matrices.

### 382 3.3.3. Unknown Input Observer Design

383 To estimate the unknown excitation force  $F_e(t)$ , it is viewed as an augmented  
 384 state to the system in Eqs. (25) and (26). Thus the augmented system can be  
 385 written as:

$$x_g = [x_{f2m} \quad F_e]^T, \quad (30)$$

$$\dot{x}_g(t) = A_g x_g(t) + B_g F_{pto}(t) + D_g \dot{F}_e, \quad (31)$$

$$y_g(t) = C_g x_g(t), \quad (32)$$

386 with

$$A_g = \begin{bmatrix} A_{f2m} & B_{f2m} \\ 0 & 0 \end{bmatrix}, \quad (33)$$

$$B_g = \begin{bmatrix} B_{f2m} & 0 \end{bmatrix}^T, \quad (34)$$

$$D_g = \begin{bmatrix} 0 & 1 \end{bmatrix}^T, \quad (35)$$

$$C_g = \begin{bmatrix} C_{f2m} & 0 \end{bmatrix}, \quad (36)$$

387 where  $x_g(t) \in \mathbb{R}^{6 \times 1}$  is the state vector of the augmented system.  $A_g \in \mathbb{R}^{6 \times 6}$ ,  
 388  $B_g \in \mathbb{R}^{6 \times 1}$ ,  $D_g \in \mathbb{R}^{6 \times 1}$  and  $C_g \in \mathbb{R}^{1 \times 6}$  are the system matrices.

389 The following UIO is adapted from [35, 36] to estimate the augmented system  
 390 state, given as:

$$\dot{x}_o(t) = P x_o(t) + G F_{pto}(t) + L y_{f2m}(t), \quad (37)$$

$$\hat{x}_g(t) = x_o(t) + Q y_{f2m}(t), \quad (38)$$

391 where  $x_o(t) \in \mathbb{R}^{6 \times 1}$  is the UIO state vector.  $P \in \mathbb{R}^{6 \times 6}$ ,  $G \in \mathbb{R}^{6 \times 1}$ ,  $L \in \mathbb{R}^{6 \times 1}$   
 392 and  $Q \in \mathbb{R}^{6 \times 1}$  are the UIO system matrices.  $\hat{x}_g(t)$  represents the estimate of  
 393  $x_g(t)$ .

394 Since the excitation force is unknown, its derivative  $\dot{F}_e(t)$  in Eq. (31) is inac-  
 395 cessible and hence viewed as a disturbance. To achieve an accurate estimation

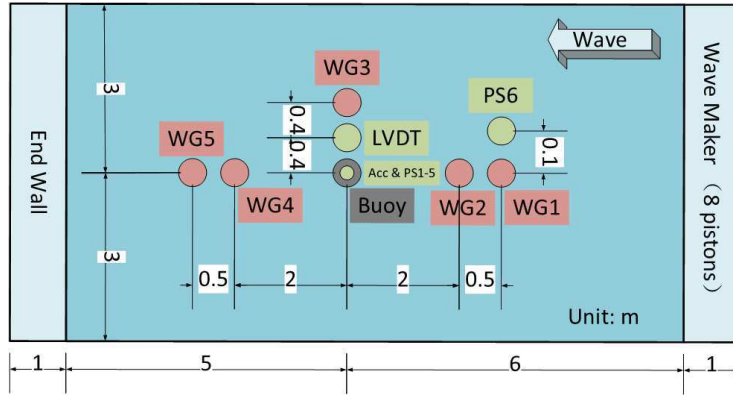


Figure 12: Sketch of the wave tank and the device installation.

396 of the excitation force, the  $H_\infty$  robust optimisation approach is applied to compute  
 397 the observer matrices  $P$ ,  $G$ ,  $L$  and  $Q$  to reject the influence of  $\dot{F}_e(t)$ , using  
 398 the MATLAB<sup>®</sup> LMI toolbox. The computation of the observer gain matrix  $L$   
 399 follows the method described in [36] and is thus omitted here.

#### 400 4. Wave Tank Tests

##### 401 4.1. Experiment Settings

402 To verify the excitation force estimations via the W2EF, PAD2EF and  
 403 UIOEF approaches, a series of wave tank tests have been conducted. As shown  
 404 in Figure 12, the wave tank is 13 m in length, 6 m in width and 2 m in height  
 405 (with water depth 0.9 m). Up to 8 pistons can be selected to generate regu-  
 406 lar/irregular waves.

407 The PAWEC is scaled down according to the Froude Number defined in  
 408 [37]. For this application the geometric ratio is selected as 1/50. Therefore, the  
 409 time ratio is 1/7.0711. For ocean waves of sea state 7 defined by the Beaufort  
 410 scale [38], its characteristics can be represented by a PM spectrum with peak  
 411 frequency  $f_p = 0.095$  Hz and significant wave height  $H_s = 4.3$  m. The scaled  
 412 down PM spectrum (according to the Froude Number) is featured by the peak  
 413 frequency  $f_p = 0.0952 \times 7.0711 = 0.67$  Hz and significant wave height  $H_s =$



414  $4.3/50 = 0.086$  m. Therefore, the wave conditions in the wave tank tests are  
415 configured with wave frequencies as  $f = 0.4 : 0.1 : 1.2$  Hz and wave height  
416  $H = 0.08$  m for regular waves. For irregular waves, the peak frequencies of the  
417 PM spectra are selected as  $f_p = 0.4, 0.6, 0.8$  Hz.

418 The 1/50 scale cylindrical heaving PAWEC has been simulated, designed and  
419 constructed for wave tank tests, model verification and control system design, as  
420 shown in Figure 12. Five Wave Gauges (WGs) are mounted to measure the water  
421 elevation in real-time, with WG1&2 in the up-stream, WG3 in line with the buoy  
422 and WG4&5 in the down-stream. For this study, only the WG3 measurement  
423 is used. WG1&2 and WG4&5 are useful to estimate the reflection of the wave  
424 tank end wall and to verify the generated irregular wave satisfies the pre-set PM  
425 spectrum. Six Pressure Sensors (PSs) are applied in the wave tank tests with  
426 PS1-5 installed at the bottom of the PAWEC to measure the dynamic pressure  
427 acting on the hull and PS6 fixed in line with WG1 for synchronisation<sup>1</sup>. A Linear  
428 Variable Displacement Transducer (LVDT) and a 3-axis Accelerometer (Acc) are  
429 rigidly connected with the oscillating body to provide motion measurements.  
430 All these sensing signals are collected by a data acquisition system connected  
431 with LABVIEW<sup>TM</sup> panel. The sampling frequency is 100 Hz. The pressure,  
432 displacement and acceleration measurements are post-processed with low pass  
433 filters to verify the modelling and estimation concepts.

434 For the *excitation tests*, the PAWEC is fixed semi-submerged and under  
435 the excitation of incident waves to verify the W2EF modelling approach. For  
436 the *wave-excited-motion tests*, the buoy is forced to oscillate from zero-initial  
437 condition under the excitation of incoming waves. Since this study has a specific

---

<sup>1</sup>The installation depth of PS6 is 0.4 m. There are two sensing systems applied: one integrated with the wave maker and the other designed for the PAWEC. It is a good idea to isolate the electrical connects of these two sensing systems in case there are some penitential conflicts. The PAWEC sensing system triggers the wave maker sensing system. However, there is still a small time shift between these two sensing systems due to different design of the hardware and software. Thus PS6 and WG1 are installed to measure the same signal to determine the time shift between these two sensing systems.

438 focus on the estimations of the excitation force, the control or PTO force is set as  
 439  $F_{pto} = 0$  N for the excitation tests or **the wave-excited-motion** tests. For control  
 440 practice,  $F_{pto}$  is known and hence it is applicable to obtain the excitation force  
 441 by subtracting  $F_{pto}$  from the estimate of PAD2EF or UIOEF approaches. If  
 442  $F_{pto}$  is not known, only the W2EF method is applicable.

#### 443 4.2. Excitation Tests

444 For the excitation tests, the PAWEC is fixed to the wave tank gantry at  
 445 its equilibrium point and excited by the incident wave. The pressure sensors  
 446 installed at the bottom of the buoy provide the measurement of the dynamic  
 447 pressure acting on the hull. Thus, the wave excitation force in heave can be  
 448 represented as:

$$F_e(t) = \iint p(t) ds \approx \pi r^2 \bar{p}(t), \quad (39)$$

449 where  $\bar{p}(t)$  represents the average value of the five pressure sensors (PS1-5).  
 450 Note that Eq. (39) only gives an simple approximation of the the excitation  
 451 force. When the buoy diameter is relative small to the wavelength (such as  
 452 tenth of the wavelength), the accuracy of Eq. (39) is acceptable. If the buoy  
 453 dimension is almost the same scale of the wavelength, more pressure sensors are  
 454 required to achieve accurate excitation force measurement.

455 Meanwhile, five WGs are installed to measure the wave elevation, amongst  
 456 which, WG3, is in line with the buoy. The measurement of WG3 represents  
 457 the incident wave at the center of the PAWEC and is adopted to provide wave  
 458 prediction in a short-term horizon  $t_c$ . A wide variety of excitation tests un-  
 459 der regular and irregular wave conditions are conducted to verify the W2EF  
 460 modelling approach. The numerical and experimental results are compared and  
 461 discussed in Section 5.1.

#### 462 4.3. Wave-excited-motion Tests

463 For the **wave-excited-motion** tests, the PAWEC is forced to oscillate from  
 464 its zero-initial condition under the excitation of the incident waves. In this

465 situation, the measurements from pressure sensors represent the total wave force  
466 rather than the excitation force, given as:

$$F_w(t) = \iint p(t) ds \approx \pi r^2 \bar{p}(t). \quad (40)$$

467 Also, Eq. (40) is valid only when the buoy dimension is relatively small com-  
468 pared with the wavelength.

469 Meanwhile, the buoy acceleration and displacement are measured by the  
470 accelerometer and LVDT, respectively. Therefore, the excitation force can be  
471 estimated via the PAD2EF approach in Eq. (22). Also, the wave elevation  
472 measurements are accessible. Thus the W2EF method can be applied on WG3  
473 measurement to approximate the excitation force according to Eqs. (14) and  
474 (15). Since the displacement measurement is accessible, the UIOEF approach  
475 in Eqs. (37) and (38) can be applied to estimate the excitation force as well.  
476 The numerical and experimental comparison of the excitation force between the  
477 W2EF, PAD2EF and UIOEF approaches is discussed in Section 5.2.

## 478 5. Results and Discussion

### 479 5.1. Results of Excitation Tests

480 Since the PAWEC is fixed during the excitation tests. The motion measure-  
481 ments are not applicable. Therefore, only the W2EF approach can be applied to  
482 estimate the excitation force. To verify the proposed W2EF modelling approach,  
483 excitation tests are conducted under regular and irregular wave conditions and  
484 the experimental data are compared with the numerical simulations of Eqs. (14)  
485 and (15).

#### 486 5.1.1. Regular Wave Conditions

487 Nine excitation tests are conducted under regular waves with wave height  
488  $H = 0.08$  m and frequencies  $f = 0.4 : 0.1 : 1.2$  Hz. For harmonic waves,  
489 precise wave prediction with  $t_c = 1$  s in advance is easy to achieve. Recall that  
490 the prediction horizon is the same as the causalisation time illustrated in Eq.

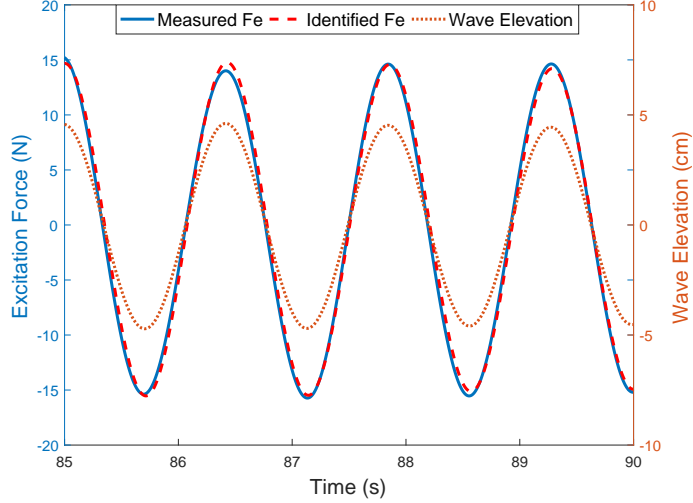


Figure 13: Comparison of the excitation forces between the measurement and the estimate via W2EF method.

491 (10) and Figure 7. Therefore, the W2EF modelling approach always provides  
 492 accurate approximation of the excitation force under regular waves. For the  
 493 harmonic wave with frequency  $f = 0.7$  Hz, the excitation force measurement in  
 494 Eq. (39) and the estimation in Eqs. (14) and (15) are compared in Figure 13.  
 495 The estimation via W2EF method shows a high accordance to the experimental  
 496 data, which indicates the validity of the W2EF method for excitation tests under  
 497 regular wave conditions.

498 To check the fidelity further, the excitation force FRF is compared with the  
 499 W2EF result as well as the NEMOH computation. The amplitude and phase  
 500 responses are shown in Figure 14 and Figure 15, respectively. The amplitude  
 501 response of the W2EF method fits the NEMOH and excitation tests data to a  
 502 high degree. This is why the analytical representations of the excitation force  
 503 in Eqs. (4) and (5) are widely adopted to investigate WEC dynamics. Note  
 504 that the excitation force amplitude response is normalised with respect to the  
 505 hydrostatic stiffness  $k_{hs}$ .

506 Figure 15 compares the experimental and numerical phase responses from

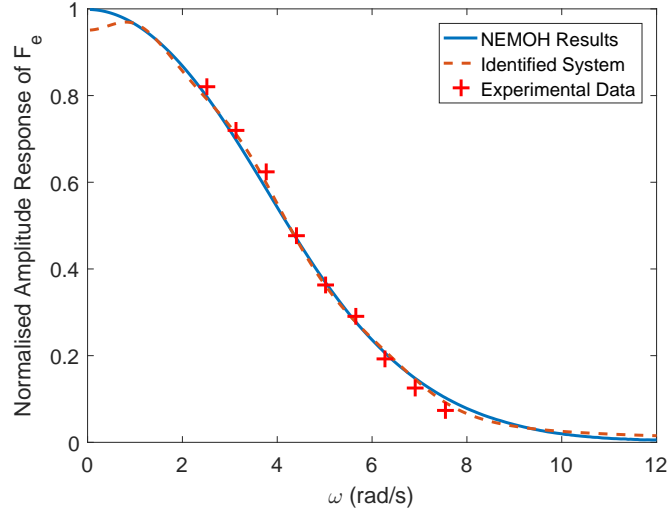


Figure 14: Amplitude response comparison of the excitation force amongst the excitation tests, NEMOH computations and W2EF simulations.

507 the incident wave  $\eta(t)$  to the excitation force  $F_e(t)$  in Eq. (9). A good accor-  
508 dance of the phase response means that the W2EF modelling approach with  
509 kernel function causlisation and wave prediction in Eq. (11) gives almost the  
510 same system description of the non-causal system in Eq. (9). Also, Figure  
511 15 illustrates that the analytical representations of the excitation force in Eqs.  
512 (4) is improper for PAWEC modelling and control design, especially when the  
513 frequency is relatively high. Note that, the excitation force phase response is  
514 normalised with respect to  $\pi$ .

### 5.1.2. Irregular Wave Conditions

516 Irregular waves characterised by the PM spectrum are adopted in the exci-  
517 tation tests and the results are shown in Figure 16. Generally speaking, the  
518 estimated excitation force via the W2EF method shows a good accordance  
519 to the experimental data for most of the time. The estimation only varies  
520 a bit from the measurement when the wave elevation is occasionally small.  
521 For instance, the identified excitation force varies from its measurement within

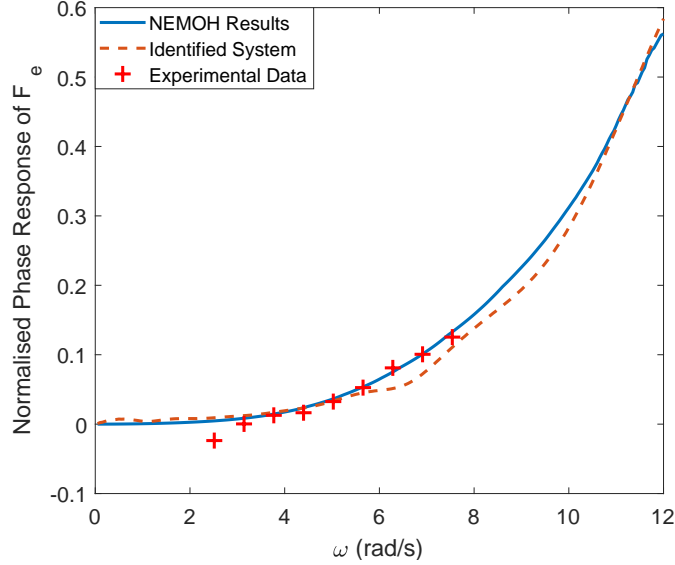


Figure 15: Phase response comparison of the excitation force amongst the excitation tests, NEMOH computations and W2EF simulations.

522  $t = 436 - 440$  s in Figure 16, case A. However, this part is not important  
 523 from the viewpoint of power maximisation. For the irregular wave condition  
 524 of  $f_p = 0.8$  Hz,  $H_s = 0.06$  m, the excitation force estimate is not as accurate  
 525 as that for the other two wave conditions. The potential reason may be the  
 526 inaccuracy in Eq. (39) since the point absorber assumption are not fully sat-  
 527 isfied. Additionally, the wave elevation predictions corresponding to Figure 16  
 528 are given in Figure 8.

### 529 5.2. Results of *Wave-excited-motion* Tests

530 For the *wave-excited-motion* tests, the PAWEC oscillates under the excita-  
 531 tion of incident waves. Therefore, the pressure, displacement and acceleration  
 532 measurements, together with the wave elevation, are available. Thus the W2EF,  
 533 PAD2EF and UIOEF approaches are adopted to approximate the excitation  
 534 force acting on the PAWEC hull. In the *wave-excited-motion* tests, the excita-  
 535 tion force is immeasurable since the pressure sensors give the total wave force

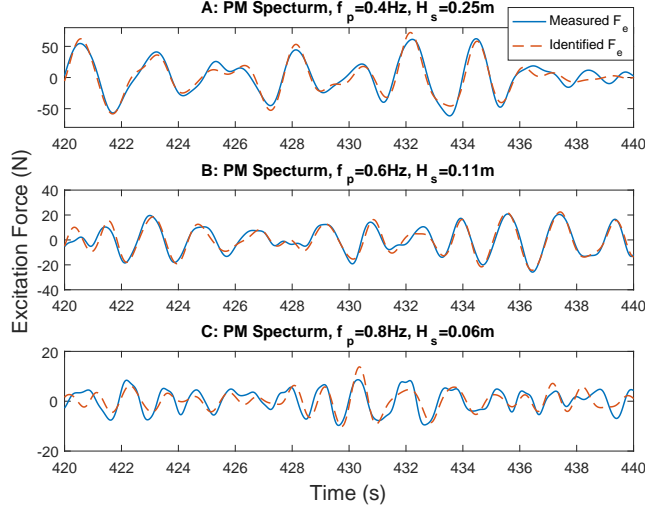
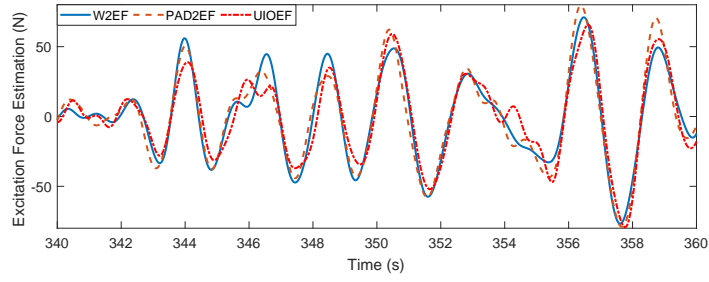


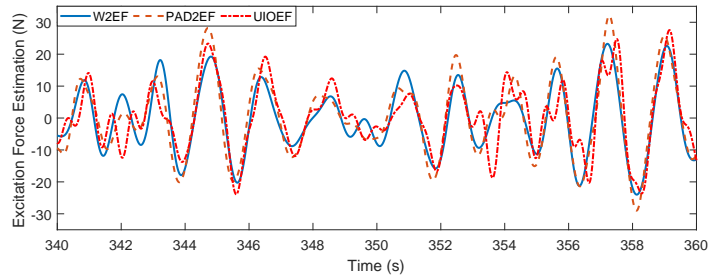
Figure 16: Comparison of the excitation force between the excitation tests and the W2EF modelling under irregular wave conditions.

536  $F_w(t)$  in Eqs. (18) and (40).

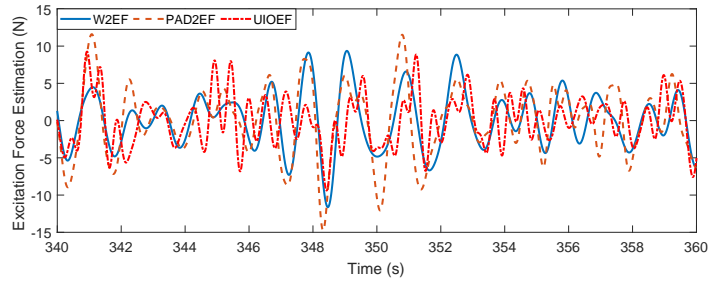
537 Three campaigns of **wave-excited-motion** tests are conducted under irreg-  
538 ular wave conditions and the excitation force comparison among the W2EF,  
539 PAD2EF and UIOEF approximation approaches is given in Figure 17. Since  
540 the excitation force cannot be measured directly, it is very hard to say which  
541 method is better. Via the comparison in Figure 17, it is found that: (i) All these  
542 three methods give good estimation of the excitation force when the wave (or  
543 excitation force) is large for the wave conditions of  $f_p = 0.4$  Hz,  $H_s = 0.25$  m  
544 and  $f_p = 0.6$  Hz,  $H_s = 0.11$  m. (ii) When the wave is small or changes rapidly,  
545 the estimations given by the PAD2EF and UIOEF approaches are more vari-  
546 able, compared with the W2EF estimation. **Compared to the excitation force,**  
547 **the radiation approximation error and non-linear friction/viscous forces [39] are**  
548 **relatively large.** (iii) Generally speaking, the magnitude of the excitation force  
549 approximation given by the W2EF method is smaller than the ones provided  
550 by the PAD2EF and UIOEF approaches. One potential reason is that the wave  
551 gauge measurement is attenuated by the interference between the incident and



(a) PM spectrum,  $f_p = 0.4$  Hz,  $H_s = 0.25$  m.



(b) PM spectrum,  $f_p = 0.6$  Hz,  $H_s = 0.11$  m.



(c) PM spectrum,  $f_p = 0.8$  Hz,  $H_s = 0.06$  m.

Figure 17: Comparison of the excitation force approximations under irregular wave conditions.



552 radiated waves [16]. (iv) For the wave condition of  $f_p = 0.8$  Hz,  $H_s = 0.06$  m, the  
553 W2EF method gives slightly better estimation than the PAD2EF and UIOEF  
554 approaches. One potential reason is that the wave excitation force is small  
555 under this wave condition and hence the mechanical friction force is relative  
556 large. The PAD2EF and UIOEF methods in this work cannot decouple the me-  
557 chanical friction force from there excitation force estimations. For the specified  
558 1/50 PAWEC, the friction can be characterised experimentally [39]. Whilst the  
559 W2EF method estimates the wave excitation force from wave measurements  
560 and hence the estimates are not affected by mechanical friction force.

561 A comparison of these methods are made as follows:

- 562 • The W2EF modelling approach requires the wave elevation measurement  
563 only. The W2EF approach shows advantages in easy implementation and  
564 good tolerance to the mechanical friction and fluid viscous forces. How-  
565 ever, the W2EF approach is subjected to linear wave theory and small  
566 radiated wave. Additionally, accurate wave prediction is compulsory to  
567 overcome the non-causality of the W2EF process.
- 568 • The PAD2EF modelling method requires the measurements of pressure,  
569 acceleration and displacement. Hence it is complex to implement. The  
570 PAD2EF estimation is affected by the modelling error of the radiation  
571 force approximation and fluid viscous force but not the mechanical fric-  
572 tion force and radiated wave. Another advantage is that the PAD2EF  
573 estimation is applicable when the incident waves are non-linear or when  
574 the W2EF process is non-linear.
- 575 • The UIOEF modelling approach only requires the displacement measure-  
576 ment. Thus it is easy to implement. Also, the UIOEF estimation does not  
577 suffer from the radiated wave but is influenced by modelling error of the  
578 radiation force approximation, the mechanical friction and fluid viscous  
579 forces. Also, the UIOEF method can be applied under the excitation of  
580 non-linear incident waves.

581 For the control structure in Figure 11, the estimation error of the excitation  
582 force will affect the power capture performance. This part of work has been  
583 investigated in [40] and it shows that the influence of the estimation error on  
584 the power capture can be attenuated at certain band of frequencies via robust  
585 control design.

## 586 6. Conclusion

587 This study focuses on the modelling of the excitation force and the model  
588 verification via wave tank tests. The excitation force can be approximated  
589 with reasonable accuracy from the measurements of wave elevation, pressure,  
590 acceleration and displacement. Therefore, the W2EF, PAD2EF and UIOEF  
591 modelling approaches are proposed, simulated and tested in a wave tank. The  
592 experimental data show a high accordance to the estimations of the W2EF,  
593 PAD2EF and UIOEF methods. However, the application scenarios of these  
594 approaches vary, as shown below:

- 595 • The W2EF method in Eqs. (14) and (15) gives reasonably accurate es-  
596 timation of the excitation force based on the conditions: (i) the incident  
597 wave is linear; (ii) the radiated wave due to the PAWEC motion is small  
598 compared to the incident wave; (iii) wave elevation measurement and its  
599 precise prediction are accessible.
- 600 • The PAD2EF approach in Eq. (22) can provide good estimation of the  
601 excitation force if the following conditions are satisfied: (i) the measure-  
602 ments of pressure, acceleration and displacement are available and (ii) the  
603 fluid viscous force is negligible.
- 604 • The UIOEF strategy in Eqs. (37) and (38) only depends on the displace-  
605 ment measurement and can provide precise estimation of the excitation  
606 force and the velocity. But the mechanical friction and fluid viscous forces  
607 cannot be decoupled from the excitation force estimation.

608 A wide variety of excitation tests and **wave-excited-motion** tests are con-  
609 ducted in a wave tank to verify the proposed excitation force approximation ap-  
610 proaches. The experimental data collected from the excitation tests fit with the  
611 W2EF model numerical results to a high degree in both time- and frequency-  
612 domains under regular and irregular wave conditions. For the **wave-excited-**  
613 **motion** tests, all the W2EF, PAD2EF and UIOEF modelling approaches are  
614 applied to estimate the excitation force and their estimations show high accor-  
615 dance to each other when buoy dimension is relatively small to the incident  
616 wavelength.

617 Therefore, these proposed excitation force approximation approaches can be  
618 useful for the performance assessment and real-time power maximisation control  
619 of WEC systems. Ongoing work focuses on the excitation force prediction and  
620 its implementation for the MPC on WEC systems.

## 621 **Acknowledgment**

622 Bingyong Guo, Siya Jin and Jianglin Lan thank the China Scholarship Coun-  
623 cil and the University of Hull for joint scholarships. Thanks are expressed to  
624 Professor Dan Parsons, Dr Stuart McLelland and Mr Brendan Murphy of the  
625 School of Environmental Sciences for their help and supervision in using the  
626 Hull University wave tank.

## 627 **Appendix**

628 The buoy dimensions are: radius  $r = 0.15$  m, height  $b = 0.56$  m, draft  
629  $d = 0.28$  m, mass  $M = 19.79$  kg, water density  $\rho = 1000$  kg/m<sup>3</sup>, gravity  
630 constant  $g = 9.81$  N/kg, hydrostatic stiffness  $k_{hs} = 693.43$  N/m and added  
631 mass at infinite frequency  $A_\infty = 6.58$  kg.

632 The system matrices of the W2EF system in Eqs. (14) and (15) are:

$$A_e = \begin{bmatrix} -0.234 & 1.818 & 0.530 & -0.554 & -0.314 & -0.054 \\ -1.818 & -0.900 & -3.043 & 1.082 & 0.861 & 0.130 \\ 0.530 & 3.044 & -1.798 & 4.233 & 1.553 & 0.306 \\ 0.554 & 1.082 & -4.233 & -2.688 & -5.096 & -0.480 \\ -0.314 & -0.861 & 1.553 & 5.096 & -3.590 & -3.064 \\ 0.054 & 0.130 & -0.306 & -0.480 & 3.064 & -0.157 \end{bmatrix}, \quad (41)$$

$$B_e = \begin{bmatrix} 164.34 & 251.36 & -236.52 & -175.67 & 114.01 & -18.71 \end{bmatrix}^T, \quad (42)$$

$$C_e = \begin{bmatrix} 1.6434 & -2.5136 & -2.3652 & 1.7567 & 1.1401 & 0.1871. \end{bmatrix}. \quad (43)$$

633 The system matrices for the identified radiation subsystem in Eqs. (20) and  
634 (21) are:

$$A_r = \begin{bmatrix} -3.1848 & -4.3372 & -3.1009 \\ 4.3372 & -0.0875 & -0.3882 \\ 3.1009 & -0.3882 & -2.8499 \end{bmatrix}, \quad (44)$$

$$B_r = \begin{bmatrix} -40.6964 & 5.9737 & 16.2722 \end{bmatrix}^T, \quad (45)$$

$$C_r = \begin{bmatrix} -0.4070 & -0.0597 & -0.1627 \end{bmatrix}. \quad (46)$$

635 The parameters of the BPF in Eq. (23) are:  $\omega_c = 8\pi$  rad/s,  $A_{bpf} = 2433$   
636 and  $Q_{bpf} = 100$ .

637 The system matrices of the UIO in Eqs. (37) and (37) are:

$$P = \begin{bmatrix} -0.57 & 9.01 & 0 & 0 & 0 & 0 \\ -27.09 & -39.1 & 0.02 & 0.02 & 0.01 & 0.04 \\ -3.24 & -0.13 & -3.18 & -4.34 & -3.1 & 0 \\ -0.95 & 0.43 & 4.34 & -0.09 & -0.39 & 0 \\ 0.2 & -1.62 & 3.10 & -0.39 & -2.85 & 0 \\ -32856 & -242450 & 0 & 0 & 0 & 0 \end{bmatrix}, \quad (47)$$

$$G = \begin{bmatrix} 0 & 0.0379 & 0 & 0 & 0 & 0 \end{bmatrix}^T, \quad (48)$$

$$L = \begin{bmatrix} 357.52 & 7881.9 & 73.80 & -158.04 & -244.25 & -9183200 \end{bmatrix}^T, \quad (49)$$

$$Q = \begin{bmatrix} -8.01 & 39.1 & -40.57 & 5.55 & 17.89 & 242450 \end{bmatrix}^T. \quad (50)$$

638 **To note:** The feedback gains of the UIO are large and sensitive to measurement  
 639 noise. It is due to the system property since the magnitude of the displacement  
 640  $z(t)$  is  $10^{-2}$  and the magnitude of the excitation force  $F_e(t)$  is 10. Thus this  
 641 is a numerical stiffness or conditioning problem with varying ratio  $10^3$ . In  
 642 real operation, a low pass filter is applied to the displacement measurement to  
 643 attenuate the noise.

## 644 References

- 645 [1] M. McCormick, Ocean wave energy conversion, Wiley-Interscience, New  
 646 York, 1981.
- 647 [2] F. d. O. Antonio, Wave energy utilization: A review of the technologies,  
 648 Renew. Sustainable Energy Rev. 14 (3) (2010) 899–918.
- 649 [3] B. Drew, A. Plummer, M. N. Sahinkaya, A review of wave energy converter  
 650 technology, P. I. Mech. A-J Pow. 223 (8) (2009) 887–902.
- 651 [4] A. Clément, P. McCullen, A. Falcão, A. Fiorentino, F. Gardner, K. Ham-  
 652 marlund, G. Lemonis, T. Lewis, K. Nielsen, S. Petroncini, et al., Wave  
 653 energy in Europe: current status and perspectives, Renew. Sust. Energ.  
 654 Rev. 6 (5) (2002) 405–431.
- 655 [5] J. V. Ringwood, G. Bacelli, F. Fusco, Energy-maximizing control of wave-  
 656 energy converters: The development of control system technology to opti-  
 657 mize their operation, IEEE Control Systems 34 (5) (2014) 30–55.
- 658 [6] S. Salter, Power conversion systems for ducks, in: Proc. of the International  
 659 Conference on Future Energy Concepts, Vol. 1, 1979, pp. 100–108.
- 660 [7] K. Budal, J. Falnes, Optimum operation of improved wave-power converter,  
 661 Mar. Sci. Commun. 3 (2) (1977) 133–150.

- 662 [8] A. Babarit, M. Guglielmi, A. H. Clément, Declutching control of a wave  
663 energy converter, *Ocean Eng.* 36 (12) (2009) 1015–1024.
- 664 [9] G. Li, M. R. Belmont, Model predictive control of sea wave energy  
665 converters—part i: A convex approach for the case of a single device, *Renew.*  
666 *Energy* 69 (2014) 453–463.
- 667 [10] G. Li, M. R. Belmont, Model predictive control of sea wave energy  
668 converters—part ii: The case of an array of devices, *Renew. Energy* 68  
669 (2014) 540–549.
- 670 [11] J. N. Newman, The exciting forces on fixed bodies in waves, *Journal of*  
671 *Ship Research* 4 (1962) 10–17.
- 672 [12] M. Greenhow, S. White, Optimal heave motion of some axisymmetric wave  
673 energy devices in sinusoidal waves, *Appl. Ocean Res.* 19 (3-4) (1997) 141–  
674 159.
- 675 [13] A. Babarit, J. Hals, M. Muliawan, A. Kurniawan, T. Moan, J. Krokstad,  
676 Numerical benchmarking study of a selection of wave energy converters,  
677 *Renew. Energy* 41 (2012) 44–63.
- 678 [14] Z. Yu, J. Falnes, State-space modelling of a vertical cylinder in heave, *Appl.*  
679 *Ocean Res.* 17 (5) (1995) 265–275.
- 680 [15] J. Falnes, On non-causal impulse response functions related to propagating  
681 water waves, *Appl. Ocean Res.* 17 (6) (1995) 379–389.
- 682 [16] G. Bacelli, R. G. Coe, D. Patterson, D. Wilson, System identification of a  
683 heaving point absorber: Design of experiment and device modeling, *Ener-*  
684 *gies* 10 (4) (2017) 472.
- 685 [17] S. Giorgi, J. Davidson, J. Ringwood, Identification of nonlinear excitation  
686 force kernels using numerical wave tank experiments, in: *Proc. EWTEC,*  
687 *Nantes, France, 2015*, pp. 09C1–1–1–09C1–1–10.

- 688 [18] B. A. Ling, Real-time estimation and prediction of wave excitation forces for  
689 wave energy control applications, Master's thesis, Mechanical Engineering,  
690 Oregon State University (2015).
- 691 [19] O. Abdelkhalik, S. Zou, G. Bacelli, R. D. Robinett, D. G. Wilson, R. G.  
692 Coe, Estimation of excitation force on wave energy converters using pres-  
693 sure measurements for feedback control, in: Proc. OCEANS MTS/IEEE  
694 Monterey, IEEE, 2016, pp. 1–6.
- 695 [20] G. Bacelli, R. G. Coe, State estimation for wave energy converters, Tech.  
696 rep., Sandia National Laboratories (SNL-NM), Albuquerque, NM (United  
697 States) (2017).
- 698 [21] M. Abdelrahman, R. Patton, B. Guo, J. Lan, Estimation of wave excitation  
699 force for wave energy converters, in: Proc. SysTol, IEEE, 2016, pp. 654–  
700 659.
- 701 [22] F. Fusco, J. V. Ringwood, Short-term wave forecasting for real-time control  
702 of wave energy converters, *IEEE Trans. Sustain. Energy* 1 (2) (2010) 99–  
703 106.
- 704 [23] M. Ge, E. C. Kerrigan, Short-term ocean wave forecasting using an au-  
705 toregressive moving average model, in: Proc. UKACC, IEEE, 2016, pp.  
706 1–6.
- 707 [24] J. Falnes, Ocean waves and oscillating systems: linear interactions including  
708 wave-energy extraction, Cambridge University Press, 2002.
- 709 [25] W. Cummins, The impulse response function and ship motions, Tech. rep.,  
710 DTIC Document (1962).
- 711 [26] G. Giorgi, J. V. Ringwood, Implementation of latching control in a nu-  
712 merical wave tank with regular waves, *Journal of Ocean Engineering and*  
713 *Marine Energy* 2 (2) (2016) 211–226.

- 714 [27] A. Babarit, G. Delhommeau, Theoretical and numerical aspects of the open  
715 source bem solver nemoh, in: Proc. EWTEC, Nantes, France, 2015, pp. 1–  
716 10.
- 717 [28] A. Roessling, J. Ringwood, Finite order approximations to radiation forces  
718 for wave energy applications, *Renewable Energies Offshore* (2015) 359–366.
- 719 [29] R. Taghipour, T. Perez, T. Moan, Hybrid frequency–time domain models  
720 for dynamic response analysis of marine structures, *Ocean Eng.* 35 (7)  
721 (2008) 685–705.
- 722 [30] S.-Y. Kung, A new identification and model reduction algorithm via sin-  
723 gular value decomposition, in: Proc. ACSC, IEEE, 1978, pp. 705–714.
- 724 [31] M. Safonov, R. Chiang, A schur method for balanced model reduction, in:  
725 Proc. ACC, IEEE, 1988, pp. 1036–1040.
- 726 [32] J. R. Halliday, D. G. Dorrell, A. R. Wood, An application of the Fast  
727 Fourier Transform to the short-term prediction of sea wave behaviour, *Re-  
728 new. Energy* 36 (6) (2011) 1685–1692.
- 729 [33] B. Fischer, P. Kracht, S. Perez-Becker, Online-algorithm using adaptive  
730 filters for short-term wave prediction and its implementation, in: Proc. 4th  
731 Inter. Conf. Ocean Energy, Vol. 1719, Dublin, Ireland, 2012, pp. 1–6.
- 732 [34] W. J. Pierson, L. Moskowitz, A proposed spectral form for fully developed  
733 wind seas based on the similarity theory of SA Kitaigorodskii, *J. Geophys.  
734 Res.* 69 (24) (1964) 5181–5190.
- 735 [35] J. Lan, R. J. Patton, Integrated design of robust fault estimation and fault-  
736 tolerant control for linear systems, in: Proc. CDC, IEEE, 2015, pp. 5105–  
737 5110.
- 738 [36] J. Lan, R. J. Patton, Integrated design of fault-tolerant control for nonlinear  
739 systems based on fault estimation and T-S fuzzy modelling, *IEEE Trans.  
740 Fuzzy Syst.* 10.1109/TFUZZ.2016.2598849, 2016.



- 741 [37] J. N. Newman, Marine hydrodynamics, MIT Press, 1977.
- 742 [38] Met Office, Exert,UK, National Meteorological Library and Archive Faxt  
743 sheet 6-The Beaufort Scale, 1st Edition, accessed: 2017-07-15.
- 744 [39] B. Guo, R. Patton, S. Jin, J. Gilbert, D. Parsons, Non-linear modelling and  
745 verification of a heaving point absorber for wave energy conversion, IEEE  
746 Trans. Sustain. Energydoi:10.1109/TSTE.2017.2741341.
- 747 [40] F. Fusco, J. Ringwood, A model for the sensitivity of non-causal control of  
748 wave energy converters to wave excitation force prediction errors, in: Proc.  
749 EWTEC, Southampton, UK, 2011, pp. 1–10.